Article

Journal of the Brazilian Chemical Society

https://dx.doi.org/10.21577/0103-5053.20230182

J. Braz. Chem. Soc. **2024**, *35*, 5, e-20230182, 1-16

Acidic and Basic Functionalized Biochar from Licuri Nutshell for Methylene Blue Removal: A More Sustainable Solution for Wastewater Treatment

Gustavo F. Bitencourt,[a,b,c] Letícia F. L. Machado,[c] Bruno S. Peixoto,[a] Laís F. de Castro,[b] Márcia Cristina C. Veloso,[a] Gilberto A. Romeiro[a] and Thiago M. Lima[*,a]

[a]*Instituto de Química, Universidade Federal Fluminense (UFF), Outeiro de São João Batista, s/n, 24020-140 Niterói-RJ, Brazil*

[b]*Laboratório de Catálise, Instituto Nacional de Tecnologia (INT), Avenida Venezuela, 82, 20081-312 Rio de Janeiro-RJ, Brazil*

[c]*Centro de Ciências Naturais e Humanas, Universidade Federal do ABC (UFABC), Avenida dos Estados, 5001, 09210-580 Santo André-SP, Brazil*

The right to clean water is one of the Sustainable Development Goals from the United Nations Agenda 2030. Industrial activity produces several tons of wastewater daily contaminated with dyes that must be treated. In this sense, the adsorption employing carbon-based materials as adsorbents is one of the most used and efficient processes. In this study, we developed a more sustainable biochar derived from a licuri nutshell (LN), a typical Brazilian lignocellulosic residue, for methylene blue (MB) removal. The chemical treatment of this biochar with sulfuric acid and sodium hydroxide created a functional structure with acid and basic sites. The licuri nutshell modified biochar (LNMB) presented a maximum adsorption capacity of MB of 826.45 mg g^{-1}, while the non-modified biochar and the commercial activated carbon presented only 5.27 and 142.86 mg g^{-1}, respectively. The recyclability of the adsorbents was evaluated, and there was a loss of efficiency in each cycle for every material. However, it is remarkable that LNMB presented in only one adsorption cycle almost six times more MB removal than the commercial material, thus proving its promising feature as a greener adsorbent derived from lignocellulosic waste.

Keywords: biochar, methylene blue, licuri nutshell, adsorption, biomass, *Syagrus coronata*

Introduction

Natural resource exploitation has been more intense in recent years to meet the demands of a growing world population.[1] Water can illustrate these natural resources, as it is essential to most human endeavors, generating a considerable amount of aqueous waste. This wastewater is released into the environment by 80% worldwide, and 95% is discarded without proper treatment in less developed countries. This has various harmful effects on the soil, sediments, and water in the area. Consequently, treating effluents is an environmental concern and has become a Sustainable Development Goals of the 2030 United Nations Agenda.[2] By focusing this study on the problem of aqueous effluents contaminated with organic compounds, some companies employ synthetic dyes and unlawfully discharge the wastewater into sewers, rivers, and oceans. For instance, the textile industry produces more than 700,000 tons of dyes yearly, and roughly 10% of this production and consumption are improperly released.[3,4]

In this sense, methylene blue (MB) is highlighted for being a substance of the class polymethine dyes, which have a chromophoric system conjugated by double bonds in an aromatic cycle, and for its cationic and basic properties.[5-7] In effluents, this compound is one of the causes of the alteration of water transparency due to its deep blue color, reducing the amount of O_2 available and, consequently, the natural photosynthetic activity of the environment. Besides, the effect of MB in concentrations near 5 ppm in angelfish left evidence of teratogenic issues, thus exposing the impacts of its acute and chronic toxicity in the ecosystems.[8] Moreover, it is known that in humans, MB can cause respiratory problems, inflammation and allergies, headache, vomiting, and mental confusion.[9]

*e-mail: tmlima@id.uff.br
Editor handled this article: Izaura C. N. Diógenes (Associate)

Thus, wastewater treatment systems have implemented various strategies to improve their operations and make them more effective, economical, and sustainable. Multiple techniques, such as advanced oxidation process (AOP), biodegradation, and phytoremediation, are already used.[7] However, the MB adsorption method is the most affordable and employs a wide range of materials, including clay minerals,[9] zeolites,[10] metalorganic frameworks (MOFs),[11] and carbonaceous materials (graphene oxides, activated carbon, and carbon nanotubes).[12] Despite these well-known adsorbents, using renewable sources for their production is essential, thus presenting a step forward in more sustainable materials. Using renewable resources like municipal solid wastes,[13] agro-industrial residues (such as rice husk, banana peel, and sugarcane filter cake),[14-16] and other abundant lignocellulosic biomass is quite promising to achieve the production of these sustainable materials.

From the point of view of a Brazilian scenario, the lignocellulosic biomass called licuri is an encouraging renewable source for adsorbent production. The licuri palm (*Syagrus coronata*), also known as "*ouricuri*" or licuri in Brazil, is recognized as one of the most valuable plants in the Caatinga region.[17] Despite the well-known uses of its fruit and almond for the food chain, fragrances, and personal care products,[18] the licuri nutshell is typically discarded since it is a resistant and non-nutritive material and is thus considered an abundant waste.[19] The total annual production of licuri fruits *per* hectare ranges from 2,000 to 4,000 tons, exposing that a generous amount of nutshell will be further discarded without any use.[20] Herein, this lignocellulosic biomass residue can be commercially upgraded using a thermochemical conversion technique to give biochar and reintegrate this residue in the circular economy of licuri palm.[21-23]

Biochar is a carbon-rich solid product that originates from the thermal transformation of organic matter at temperatures above 250 °C and in a low-oxygen atmosphere. The initial focus of biochar production was to improve soil fertility and nutrient retention in plants and reduce N_2O, CH_4, and CO_2 emissions.[24] Through technological advances, the use of biochar went far beyond these applications, where methods of treating and activating biochars (base-KOH, K_2CO_3, NaOH, and acid-H_2SO_4, H_3PO_4, and HCl) to control the surface chemistry and physical properties towards effective adsorption of contaminants are being discussed.[25-27] However, it is noteworthy that biochars with both acidic and basic properties remain relatively underrepresented in the existing literature. This knowledge gap is particularly conspicuous in the realm of catalysis and adsorption processes, which need the presence of both Brønsted and Lewis sites for enhanced reactivity.[28,29] The coexistence of acidic and basic functional groups on biochar surfaces holds substantial promise, as it allows selective adsorption and targeted reactions with specific molecules, contingent upon their charge and chemical characteristics.[30] This inherent selectivity emerges as a valuable asset, especially in scenarios involving complex mixtures of contaminants in water or when aiming to optimize the production of a specific compound within a catalytic reaction.

Furthermore, the suitability of biomass waste-derived biochar to more extensive scale and the life cycle assessment (LCA) also has been a vital topic to boost the implementation of these carbon materials in industrial applications.[31] For example, Gaunt and Lehmann[32] studied the environmental benefits of biochar addition to agricultural soils and compared its use to energy generation. They found that biochar had to be priced at US$47 *per* ton to compensate for potential economic profits from additional energy generation, emphasizing its potential as a soil amendment. Similarly, Peters *et al*.[33] modeled a slow pyrolysis system for biochar production from lignocellulosic feedstocks and observed harmful greenhouse gas emissions indicating of significant carbon abatement potential. Nonetheless, Choudhary and Philip[34] showed that acid-modified biochar, applied to wastewater treatment, had a total impact contribution of 20 times less than commercial activated carbon in the LCA, demonstrating a more favorable performance in climate change mitigation and low-cost adsorbent. These studies collectively highlight biochar's role in the sustainable aspect of climate change mitigation while emphasizing the economic considerations associated with its various applications.

Thus, this study explores the valorization of the licuri nutshell through slow pyrolysis and also evaluates a chemical treatment in the generated biochar toward removing MB dye from aqueous solutions. The adsorption was drastically increased when the biochar was modified with sulfuric acid and sodium hydroxide due to the creation of acid and basic surface groups. All the materials prepared were analyzed regarding their physicochemical properties, and the chemically treated biochar was extensively studied in the MB removal, i.e., equilibrium curves, kinetics, and adsorption mechanisms. The comparison with commercial activated carbon and other materials in the literature revealed that this modified biochar presented an outstanding capacity for MB removal, being suitable for wastewater treatment and incorporating a more sustainable feature into the process.

Experimental

Chemicals

All chemicals used were analytical grade quality and used without further purification. Methylene blue (empirical formula: $C_{16}H_{18}ClN_3S$) was purchased from Sigma-Aldrich (Cotia, Brazil). Sulfuric acid, sodium hydroxide, sodium carbonate, sodium bicarbonate, and chloridric acid were purchased from Synth (São Paulo, Brazil). Commercial activated carbon was purchased from Dinâmica (Indaiatuba, Brazil).

Sampling and biochar production

The licuri nutshell (LN) was collected from a local community in Caldeirão Grande, Bahia, Brazil (11°0'32''S and 40°18'7W). The raw biomass was dried overnight (105 °C) and processed in a ball milling.[35] A commercial activated carbon, labeled as CAC, was used as a comparative material for the adsorption tests. This carbon was dried at 105 °C for 12 h and received a granulometric adjustment between 0.212 and 0.045 mm.

According to previous studies of our research group,[15,35,36] 250 g of raw biomass were subjected to the thermochemical process in a batch-type reactor using a Heraeus R/O 100 oven (Niterói, Brazil). The sample was positioned in the central region of the tube, being isolated from the rest of the system by a layer of glass wool at the terminals of the tube to allow only the passage of gases. A continuous flow of N_2 gas at 500 mL min^{-1} was applied for 10 min before the pyrolysis and throughout the process to ensure an inert atmosphere. After this purging, the heating started at 12 °C min^{-1} until 400 °C and kept at this temperature for 90 min. The biochar was collected, and the other products formed in the pyrolysis (aqueous phase and bio-oil) were reserved. After the pyrolysis process, the licuri nutshell biomass (LN) was named licuri nutshell biochar (LNB).

Chemical treatment of biochar

For the acid modification, a mixture of biochar (LNB) and H_2SO_4 (mass ratio 1:2) was heated at 185 °C for 3 h under stirring.[36] Then, small amounts of distilled water were added to the mixture to ensure the system's homogeneity. The mixture was cooled until room temperature and washed with distilled water. Subsequently, the solid was soaked in a 10% NaOH solution for 30 min under stirring and washed with distilled water until pH = 7. The resultant solid was dried overnight (105 °C), and the LNB sample was converted into the licuri nutshell modified biochar (LNMB).

Physicochemical characterization of the materials

Ultimate analysis (CHNS)

The CHNS analysis was performed using FlashEA 1112 equipment (ThermoScientific, Rio de Janeiro, Brazil) in triplicate, and the standards used were 2,5-bis(5-*tert*-butyl-benzoxazol-2-yl)thiophene and L-cystine. The oxygen content was obtained by difference according to equation 1.

$$O\ (\%) = 100 - (C + H + N + S) \quad (1)$$

where O, C, H, N, and S are the percentage weight of each element.[37]

Proximate analysis

The moisture, volatile matter, and ash content were performed in duplicate according to ASTM 1762-84.[38] In addition, the fixed carbon content was determined indirectly from moisture, volatile matter, and ash content values, as described in the ASTM D3172-13.[39]

Thermogravimetric analysis (TGA)

The thermogravimetric studies were performed in a DTG-60/60H (Shimadzu, Niterói, Brazil) equipment for air atmosphere and a STA 409 PC/PG equipment (Netzsch, Niterói, Brazil) for N_2 atmosphere. For these analyses, 6 mg of each sample were weighed in a platinum crucible. The analysis parameters were the heating rate at 10 °C min^{-1} under a flow rate of 50 mL min^{-1} of gas until a temperature of 800 °C for air and 500 °C for N_2.[40]

Scanning electron microscopy (SEM)

Micrographs were performed in a scanning electron microscope QUANTA FEG 450 (FEI, Santo André, Brazil). The samples were dispersed in isopropanol, kept in an ultrasonic bath for 30 min, followed by a dispersion over a 12 mm carbon conductive tape, and then dried. A 20 nm Au sputtering coating was used to enhance the conductivity of samples. The ImageJ[41] software was used to analyze the cavities in the micrographs. Twenty regions in each material (LNB and LNMB) were measured and expressed as their mean and standard error value.

Textural characterization

The textural analysis using N_2 sorption was performed in Autosorb-1 (Quantchrome, Santo André, Brazil) equipment. The materials were treated in a vacuum at 150 °C for 24 h before the analysis. The pore distribution and total pore volume were determined by the Barrett-Joyner-Halenda (BJH) method, and the surface area was

calculated using the Brunauer-Emmett-Teller (BET) method from $P/P_0 = 0.05$ until 0.30.[42]

Fourier-transform infrared spectroscopy (FTIR)

Infrared spectra were made from 550 to 4000 cm^{-1} in a spectrometer (Nicolet iS50 FTIR- Niterói, Brazil) using a direct insertion method of the sample in the attenuated total reflectance (ATR) with 16 scans. All samples were dried to obtain a spectrum without moisture interferences.

Boehm titration

The Boehm titration method was used to quantify the basic and acid groups on the surface of the carbonaceous material.[43,44] Three hundred milligrams of each adsorbent were suspended in 25 mL of four different solutions: (*i*) 0.0990 mol L^{-1} NaOH solution to determine the total acid groups and phenolic groups, (*ii*) 0.1003 mol L^{-1} Na_2CO_3 solution to determine the lactonic groups and, (*iii*) 0.0996 mol L^{-1} $NaHCO_3$ solution to determine the carboxylic groups, and (*iv*) 0.0972 mol L^{-1} HCl solution to determine the total basic groups.[45] The suspensions were kept under agitation in an orbital shaker (24 h, 150 rpm) and centrifuged. Then, 5 mL aliquots of the supernatants were taken, diluted to 30 mL, and titrated with a 0.096 mol L^{-1} HCl standardized solution for the acid groups quantification. The aliquots were titrated with a standardized NaOH solution for the basic groups quantification. The titrations were performed in triplicate, and the results were reported as mean with standard error.

Surface charge measurements

A Zetasizer NanoZS equipment (Malvern, Santo André, Brazil) was used to measure the zeta potential of the carbonaceous solids produced from licuri nutshell. The samples were prepared as described: 5 mg of each adsorbent were suspended in 25 mL of deionized water from pH = 3 to 12 (adjustments with 1-0.01 mol L^{-1} NaOH and HCl), and the suspensions were stirred in an orbital shaker (24 h and 150 rpm). After that, these samples were sonicated for 30 min, and 1.3 mL aliquots of each solution were measured.[46]

Adsorption studies of methylene blue (MB)

Different experimental variables were studied for the adsorption tests of MB, except for temperature variation and adsorbent amount. In the kinetic studies, solutions of MB were used in the following concentrations: 10, 25, 376, and 1376 mg L^{-1}.[47] The contact time ranged from 2 min to 24 h to obtain the optimum equilibrium time of the materials. The effect of pH in the adsorption of MB was evaluated by changing the pH of a previously made dye solution and adjusting it with 1 mol L^{-1} of NaOH or HCl.

The effect of the dye concentration was evaluated in a preliminary adsorption experiment on LNB and LNMB using aqueous solutions of MB at low concentrations (0.5-14.0 mg L^{-1}). In the subsequent experiments, the concentrations ranged from 10 to 1187 mg L^{-1} and were also used for the isotherm study. During all tests, 10 mg of each material was used, with particle size between 0.212 and 0.045 mm, for 10 mL of each MB solution (dosage of adsorbent 1 g L^{-1}). The tests kept the material in contact with the MB solutions in an orbital shaker Q225M (Quimis, Niterói, Brazil) with constant agitation at 150 rpm, at room temperature 20 ± 2 °C. After adsorption, the samples were centrifuged at 3600 rpm for 2 min to separate the suspended char from the solution. Next, 5 mL aliquots of the supernatant were removed to analyze the resulting absorbance in the UV-Vis spectrophotometer (PerkinElmer Lambda 45, Niterói, Brazil). The maximum wavelength of the MB used in the measurements was 665 nm. The calculation used for quantifying the adsorptive capacity is represented by equations 2 and 3.

$$q_e = \left(\frac{C_0 - C_e}{m}\right)V \tag{2}$$

$$\text{Removal of MB}\,(\%) = \left(\frac{C_0 - C_e}{C_0}\right) \times 100 \tag{3}$$

where q_e (mg g^{-1}) is the adsorptive capacity at equilibrium, C_0 (mg L^{-1}) is the solution concentration at the beginning of the experiment, C_e (mg L^{-1}) is the solution concentration at equilibrium, V (L) is the solution volume and m (g) the adsorbent mass. The kinetic study uses pseudo-first-order (PFO), pseudo-second-order (PSO), and adsorption rate models to characterize the phenomena on the adsorbent surface.[48-51] These models were used in their linear forms, respectively, according to equations 4-6.

$$\log\left(q_e - q_t\right) = \log q_e - \left(\frac{k_1}{2.303}\right)t \tag{4}$$

$$\frac{t}{q_t} = \left(\frac{1}{k_2 q_e^2}\right) + \left(\frac{1}{q_e}\right)t \tag{5}$$

$$h = \frac{q_t}{t} = k_2 q_e^2 \tag{6}$$

where t (min) is the contact time of the solution with the adsorbent, q_e, and q_t (mg g^{-1}) are the amounts of MB adsorbed at equilibrium, and time t, k_1 (min^{-1}) is the pseudo-

first-order adsorption rate constant, k_2 (g mg^{-1} min^{-1}) is the pseudo-second-order adsorption rate constant, and h (mg g^{-1} min^{-1}) is the adsorption rate.

The linear Langmuir and Freundlich (equations 7 and 8) arranged below were the isotherm models used to describe the adsorption process.[48]

$$\frac{C_e}{q_e} = \left(\frac{1}{q_{max}}\right)C_e + \left(\frac{1}{q_{max}K_L}\right)t \quad (7)$$

$$\log q_e = n\log C_e + t\log K_F \quad (8)$$

where K_L is the Langmuir constant (L mg^{-1}), K_F is the Freundlich constant (mg g^{-1}), C_e is the concentration in solution at equilibrium (mg L^{-1}), q_e is the adsorptive capacity at equilibrium (mg g^{-1}), q_{max} is the monolayer maximum adsorption capacity of the material (mg g^{-1}).

An ethanol-washing procedure was used to remove the adsorbed MB from the materials for the recyclability tests. After each adsorption cycle, about 50 mL of absolute ethanol was added into the material recipient and sonicated for 1 h until the color of the solution became blue. Then, the supernatant was removed, and another washing started until the ethanol became almost colorless. After the last washing with ethanol, the same procedure was repeated with deionized water, followed by the sample being dried overnight at 100 °C for the next adsorption cycle.[52]

Results and Discussion

Slow pyrolysis of licuri nutshell

The slow pyrolysis process of the licuri nutshell (LN) produces biochar as the primary product (36%) (Figure S1, Supplementary Information (SI) section). In addition, it was also detected pyrolysis gas (24%), an aqueous fraction (31%), and bio-oil yield (9%).[22] From a more sustainable point of view, the gaseous fraction might be recycled as a carrier gas or even for energy purposes such as heat generation. In addition, the aqueous fraction might be redirected to studies of biological activity against pests and microorganisms and even for the production of biofuels, thus adding a valuable purpose to these other products.[53-55]

Physicochemical characterization of the materials

The ultimate and proximate analysis results for the studied biochars are presented in Table 1. As expected, carbon was the most significant fraction of LN, LNB, and LNMB materials as it is the most abundant in the lignocellulosic materials. The H/C molar ratio represents the aromaticity degree (balance between aliphatic carbon and aromatic compounds), in which the values reported in the literature for raw lignocellulosic biomass is 1.72, and for pure cellulose is 1.67.[56] Therefore, due to the pyrolysis process leading to partial thermal decomposition of the organic content, dehydration, dehydrogenation reactions, and the cleavage and cracking of weak hydrogen bonds within the biochar structure, these are expected to possess a lower degree of aromaticity.[57,58] In this sense, the raw LN was the material that presented the highest H/C ratio (1.36), while its derived biochar products were 0.56 for LNB and 0.63 for LNMB, showing the effect of the transformations (pyrolysis and chemical treatment).[56]

As for the H content, it can be observed that it follows a decreasing pattern as the raw material was

Table 1. Results of ultimate analysis and proximate analysis for the produced biochars

Property	Material			
	LN	LNB	LNMB	CAC
C / %	45.24 ± 1.01	69.44 ± 0.22	52.07 ± 0.58	72.47 ± 0.58
H / %	5.11 ± 0.11	3.24 ± 0.07	2.74 ± 0.10	1.24 ± 0.14
N / %	0.73 ± 0.02	0.71 ± 0.01	0.46 ± 0.01	0.44 ± 0.08
S / %	ND	ND	ND	ND
O[a] / %	48.92 ± 0.95	26.61 ± 0.15	44.73 ± 0.58	25.85 ± 0.37
Molar ratio H/C	1.36	0.56	0.63	0.21
Molar ratio O/C	0.81	0.29	0.64	0.27
Moisture / %	10.1 ± 0.14	0.9 ± 0.21	2.7 ± 0.03	0.3 ± 0.01
Volatile matter / %	66.8 ± 1.87	25.9 ± 0.16	32.5 ± 0.96	7.2 ± 0.23
Ash content / %	2.4 ± 1.48	6.7 ± 0.12	18.5 ± 0.63	15.9 ± 0.08
Fixed carbon / %	20.7 ± 0.25	66.4 ± 0.17	46.4 ± 1.5	76.6 ± 0.30

[a]It was calculated by difference accordingly to equation 1. ND: not detected; LN: licuri nutshell; LNB: licuri nutshell biochar; LNMB: licuri nutshell modified biochar; CAC: commercial activated carbon.

transformed through pyrolysis. This occurs because of the volatilization and decomposition reactions in the lignocellulosic biomass, so the H is linked to the volatile and heavier compounds formed and subsequently condensed or released as pyrolysis gas.[59] The decrease after the chemical treatment of the biochar LNB, i.e., the LNMB material, is related to the oxidation of the biochar's structure through H_2SO_4, which increases its O content and therefore decreases the others, such as H.[57] The N content follows the same pattern of increase in the transformations of the raw biomass since is more likely to be retained in the biochar's structure compared with the oxygenated fractions. This observation is associated with the higher chemical stability of N, compared to O, when conjugated or interacting with aromatic substances and functional groups, which are present in more significant amounts in the lignocellulosic carbonaceous matrix.[60] Another critical point to be mentioned in the N content is the environmental issues related to releasing NOx gases, thus contributing to atmospheric pollution. These gases (NO and NO_2) are formed during the combustion of certain materials at high temperatures. In the long term, they end up being more harmful than SOx and also prejudice the photosynthesis of various living beings, reducing the amount of O_2 available in the air.[1,60,61] Thus, nitrogen contents of materials from licuri did not change significantly (0.73, 0.71, and 0.46%). They were close to the reference commercial carbon (0.44%), indicating its application for other environmental purposes and not affecting the atmosphere with the release of NOx during their production. The sulfur content in materials content has demonstrated significant importance to concerns relating to climate change.[62] Besides, all licuri nutshell-derived materials, including the LNMB treated with H_2SO_4, exhibit this beneficial environmental aspect by not retaining sulfur in their composition.[63]

It is essential to mention that the combination of oxygen and carbon content provides the molar ratio of O/C, typically used to represent the amount of oxygenated functional groups. This ratio might be associated with the adsorption capacity of these biochars.[61] However, when analyzing the O/C ratio of LN (0.81), LNB (0.29), and LNMB (0.64), it can be seen that pyrolysis reactions removed a large part of these oxygenated groups from the raw biomass, which might represent a harmful effect for the final material LNMB. The proximate analysis furnishes essential insights into the modulation of the adsorption capacity, such as the ash content and volatile matter.[64] In the studies reported by Niu *et al.*,[64] the best ability in MB removal was observed for the material with the highest ash content, volatile matter, and oxygen content among the biochars. Thus, it is also reported that the evolution of some gases during pyrolysis and H_2SO_4 impregnation act as pore development and incorporation of oxygenated functional groups, consequently increasing adsorption properties through different mechanisms.[65]

Successive, the thermal behavior of the produced carbonaceous materials was evaluated under nitrogen (Figure 1a) and synthetic air (Figure 1b), and the decomposition data are presented in Tables S1-S2 (SI section).

The TGA analysis under an inert atmosphere (N_2) was made to simulate the pyrolysis process and observe these materials' thermal stability. In Figure 1a, the first weight loss event from 25-105 °C is assigned to the loss of humidity and volatile organic molecules adsorbed on the materials. Also, it is notable that LN shows four weight loss events, while LNB and LNMB presented three and two events, respectively. This can be associated with the decomposition of the lignocellulosic structure, which is more pronounced in raw biomass. Also, LNB showed a considerable weight loss from 275-500 °C (71%), while LNMB was more

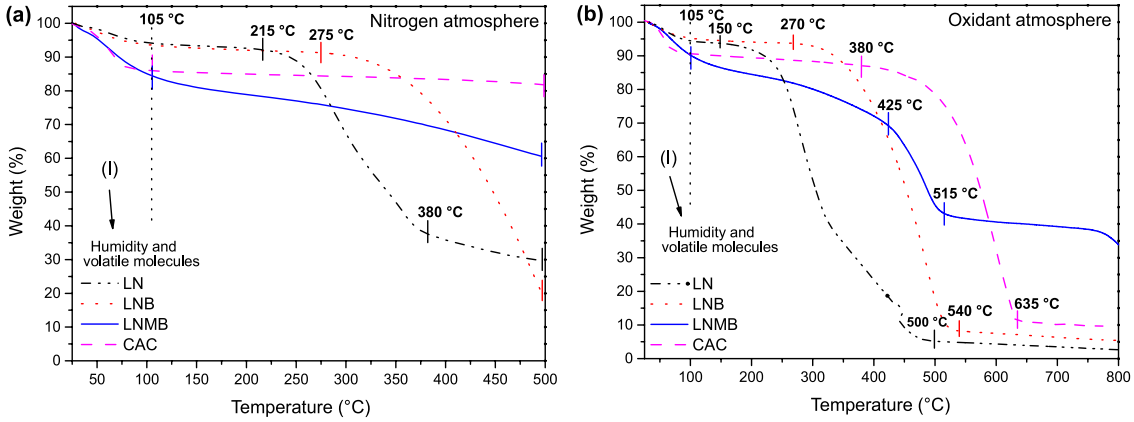

Figure 1. Thermogravimetric decomposition curves of studied materials. (a) Atmosphere: nitrogen. (b) Atmosphere: synthetic air (oxidant). LN: licuri nutshell; LNB: licuri nutshell biochar; LNMB: licuri nutshell modified biochar; CAC: commercial activated carbon.

thermally stable, showing a slightly constant decrease from 105-500 °C, ending in 24% of weight loss. When comparing the raw biomass LN with the biochars LNB and LNMB, it is possible to note that pyrolyzed materials possibly present a higher amorphous carbon degree due to the thermochemical treatments made in this work (pyrolysis and acid-base modification), justifying their lower weight loss from 250-350 ºC due to lesser depolymerization of cellulose, which is responsible for creating the arrays of amorphous carbon.[66] The thermal behavior under an oxidant atmosphere (Figure 1b) is helpful to examine the stability of the materials under more real circumstances since the adsorption capabilities of these biochars will be evaluated under a non-controlled atmosphere.[67] It can be observed that all samples presented stability at temperatures indicated by region (I) in the graphs. This stability under an air atmosphere at this temperature range is required since the adsorption of contaminants in aqueous effluents occurs at lower temperatures.[68] As expected, the raw biomass LN presented the lowest thermal stability with a weight loss higher than 90% starting at 150 °C and almost completely decomposed at 500 °C. The biochar produced from licuri nutshell LNB presented significantly higher thermal stability, and its decomposition occurred in the 270-540 °C range. In addition, the modified biochar LNMB presented a weight loss event from 105 to 425 °C, assigned to the decomposition of oxygenated compounds created in the chemical impregnation process. A second weight loss event from 425 to 515 °C was also observed for this material and assigned to the decomposition of organic matter. It is worth mentioning that LNMB presented the highest ash content and thus presented thermal stability from 515 to 750 °C.[69] The commercial activated char presented the highest thermal stability among all the materials, with the decomposition event assigned to organic matter starting at 380 °C and ending at 635 °C.

The morphological characterization of the studied carbonaceous materials was performed using SEM, as shown in Figure 2. From these images, it is possible to note a significant difference in the morphological characteristics of these materials. The raw biomass LN presented a thin fibrous husk morphology with irregular cavities. After pyrolysis, LNB showed a granular aspect and a homogeneous surface with few rugosities and a small number of cavities with a mean size of 6.7 ± 2.8 µm. In contrast, after the chemical treatment with H_2SO_4 and NaOH, the LNMB presented a distinct surface morphology from its precursor material LNB. It is possible to identify some larger cavities, within a mean size of 13.5 ± 4.7 µm, in different layers of the material and a considerable increase in the number of other smaller cavities (1.0 ± 0.4 µm), which is possibly related to the surface's corrosion. The reactions responsible for this oxidation of the material can be elucidated through the dehydration reaction of the carbonaceous matrix of biochars with H_2SO_4, which facilitates the formation of internal pores, cavities, and oxygenated functional groups.[70] Meanwhile, the CAC image furnished an intermediate surface between LNB and LNMB, presenting a regular structure and well-developed pores.[13,71-73]

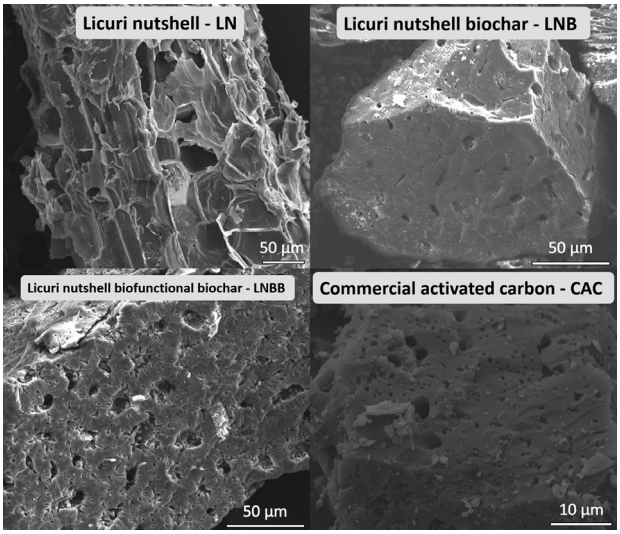

Figure 2. SEM images of all adsorbents studied.

The FTIR spectra are presented in Figure 3. A typical lignocellulosic biomass spectrum was observed for the precursor material (LN), suggesting a prominent band in the 3400-3200 cm^{-1} range related to O–H stretching of alcohols or carboxylic acids. In 1690 cm^{-1}, a low-intensity band related to C=O stretching can be noted, and an intense stretching of C=C bond at 1610 cm^{-1}. In addition, three bands at 1364/1240/1030 cm^{-1} associated with C–O in esters, carboxylic acids, or ketones were observed.[74] Comparing this raw biomass LN to its pyrolyzed-derived material (LNB), an intensity decrease in all bands related to O bonds is noticeable. This decrease is assigned to many volatile and structural oxygenated compounds transformed during pyrolysis at 400 °C.[66] Furthermore, the bands associated with C=O and C–O stretching can still be seen (1690 and 1364 cm^{-1}) in the LNB sample. After the chemical treatment of LNB, it can be observed on LNMB an increase in the bands assigned to oxygenated functional groups stretching due to the high oxidant activity of sulfuric acid and a large band at 3400-3200 cm^{-1} associated with O–H stretching and C–O stretching bands at 1364/1190/1033 cm^{-1} also reappeared.[52] As for commercial activated carbon, low-intensity signals of superficial functional groups can be seen and assigned to C–H, C=C,

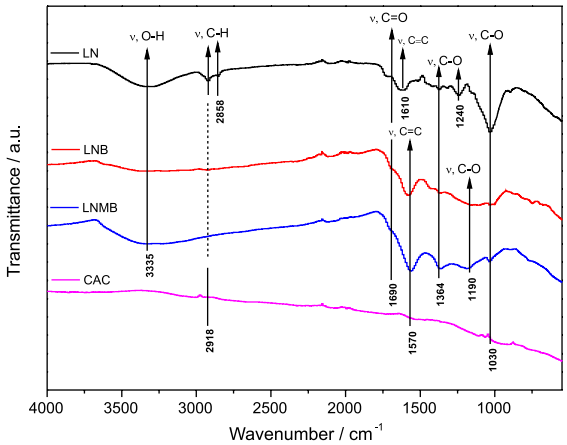

Figure 3. Normalized FTIR (ATR) spectra of the materials studied. LN: licuri nutshell; LNB: licuri nutshell biochar; LNMB: licuri nutshell modified biochar; CAC: commercial activated carbon.

and C–O vibrational bands at 2918, 1570, and 1030 cm^{-1}, respectively.[75]

As seen in Table 2, the textural characterization using N_2 physisorption (specific surface area, S_a, pore volume V_p, and pore size, Dp) of the licuri nutshell-derived materials did not show a considerable change between the pyrolysis and the chemical treatment. It can be noted that all the licuri nut-shell-derived samples had low surface areas (< 2 $m^2 g^{-1}$) and a similar total pore volume and size (0.010-0.012 $cm^3 g^{-1}$ and 4.9-17.2 nm, respectively).[76,77] These results indicate that the conditions used for the chemical treatment acted more superficially, not developing a highly porous material. The N_2 adsorption isotherms are presented in Figure S2 (SI section). LN, LNB, and LNMB are classified as type II, characteristic of non-porous or microporous materials with low interaction with N_2 molecules, as suggested by the less distinct B points.[78] Moreover, the isotherm of the commercial activated carbon is classified as a mixture of type I and IV characteristic of the presence of micro- and mesopores and hysteresis loop classified as H4-typical of micro-mesoporous carbons.[78]

Following, the quantification of surface functional groups of these materials was accessed using Boehm titration.[73,79] The results indicated an improvement of the total acid sites from 1.52 (LNB) to 2.67 (LNMB) mmol g^{-1} due to the H_2SO_4 treatment, which successfully incorporated oxygenated-containing functional groups.[80] LNMB showed 1.68, 0.24, and 0.75 mmol g^{-1} of phenolic, carboxylic, and lactonic functional groups, respectively. The total basic sites were also highly increased from 0.23 (LNB) to 2.96 (LNMB) mmol g^{-1} during the NaOH washing process, achieving a material with dense coexisting areas with properties ranging from acidic to basic.[74] It is important to remark that, instead of merely rinsing it with water to remove any residual acid, NaOH also facilitates the formation of other active sites, enhancing the adsorption process. One of the reasons for this can also be attributed to the fact that NaOH treatment can break chemical bonds such as alkyl-aryl in the carbonaceous structure in addition to dehydration reactions, enabling the formation of $–C–O^-Na^+$ and $–C–O^-$ sites on the surface.[81] Furthermore, it is essential to highlight that the acidity of the material could be even higher. Still, because of this alkaline washing to insert the basic groups, the biochar has part of its acidic surface groups being neutralized throughout the process.[82] In contrast, the commercial activated char CAC has not presented appreciable acid sites and total basic sites of 0.57 mmol g^{-1}.

Adsorption studies of methylene blue

Adsorption kinetics

The adsorption kinetics studies of MB on LN-derived biochars and commercial activated carbon were first performed at 10 mg L^{-1} (lower concentration) and then at

Table 2. Textural and chemical surface properties of the studied materials

Property	Material			
	LN	LNB	LNMB	CAC
S_a / ($m^2 g^{-1}$)	0.8	1.5	0.5	645.9
V_p / ($cm^3 g^{-1}$)	0.013	0.010	0.012	0.286
Dp / nm	4.9	17.2	5.6	3.2
Total basic sites / (mmol g^{-1})	0.11 ± 0.03	0.23 ± 0.03	2.96 ± 0.01	0.57 ± 0.03
Total acid sites / (mmol g^{-1})	2.24 ± 0.14	1.52 ± 0.02	2.67 ± 0.09	0.0
Phenolic groups / (mmol g^{-1})	1.97 ± 0.15	1.07 ± 0.16	1.68 ± 0.10	0.0
Carboxylic groups / (mmol g^{-1})	0.13 ± 0.09	0.39 ± 0.20	0.24 ± 0.09	0.0
Lactonic groups / (mmol g^{-1})	0.14 ± 0.07	0.06 ± 0.02	0.75 ± 0.01	0.0

S_a: specific surface area; V_p: pore volume; Dp: pore size; LN: licuri nutshell; LNB: licuri nutshell biochar; LNMB: licuri nutshell modified biochar; CAC: commercial activated carbon.

higher concentrations (25, 376, and 1376 mg L^{-1}). Figure 4a presents the adsorption behavior at the same 10 mg L^{-1} of MB concentration for all materials. LNB adsorption rate was lower until 3 h and reached the equilibrium at 24 h (h = 10 mg g^{-1} h^{-1}).[83] The adsorption process was much faster for the LNMB and CAC carbons, almost reaching the equilibrium at 0.25 h, which justifies their elevated adsorption rate (h = 854.7 and 595.2 mg g^{-1} h^{-1}, respectively). In this sense, the kinetics evaluation at higher concentrations was carried out due to the almost complete removal of MB. In Figure 4b can be seen that the adsorption capacity of all materials gradually increases until 10 h, and then slowly reaches the equilibrium at 24 h. This phenomenon is explained by the pronounced availability of surface groups or active sites (as observed in Table 2) at the beginning of the adsorption process. Then, when these sites were almost saturated, the adsorption tended to decrease until they reached their maximum adsorption capacity.[83] In this context, LNB, LNMB, and CAC achieved an adsorption capacity (q_e) of 18.9, 979, and 190 mg g^{-1} at 24 h, respectively.

The kinetic modeling for these materials is presented in Table 3, with more details in Figures S3-S5 and Tables S3-S5 (SI section). All materials better fit the PSO since the R^2 values were closer to 1 at lower and higher concentrations. In contrast, the PFO presented adjustment values relatively lower than 1, suggesting that the PSO model was more accurate in describing the adsorption process. Since the calculated adsorption capacity (q_{calc}) values were very close to q_e values (with discrepancies lower than 5%), the PSO model indicates that the adsorption has a rate-limiting step mainly occurring through the physicochemical interactions of the adsorbent surface and the adsorbate.[64,84]

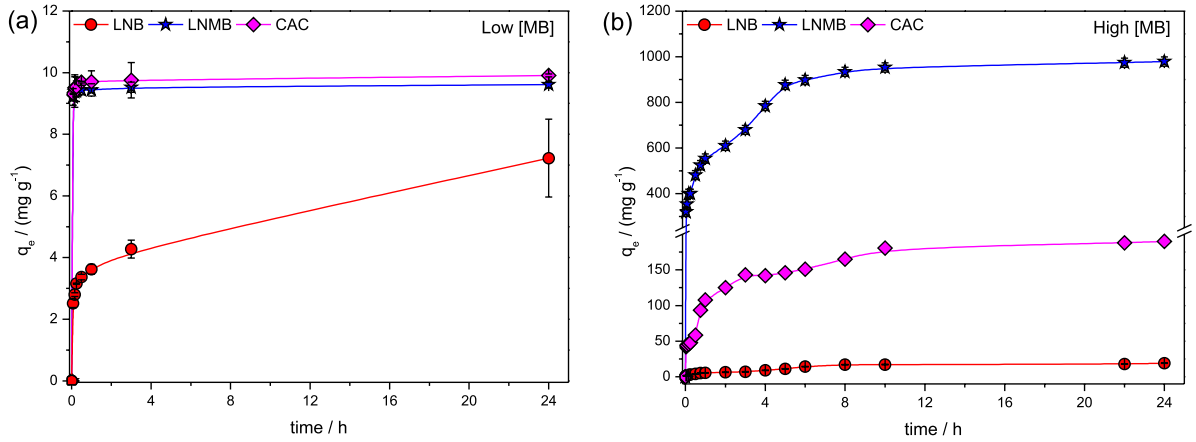

Figure 4. (a) Kinetic study of the materials in MB solutions at 10 mg L^{-1} (lower concentration). (b) Kinetic study of the materials in MB solutions at 25, 376, and 1376 mg L^{-1} for LNB, LNMB, and CAC (higher concentrations). Conditions: mass of adsorbent = 10 mg, volume of dye solution = 10 mL (dosage 1 g L^{-1}), T = 20 °C, pH = 6, and 150 rpm.

Table 3. Kinetic parameters of methylene blue (MB) adsorption for the studied carbonaceous materials at lower and higher MB concentrations

Sample	Kinect model	R^2	q_e / (mg g^{-1})	q_{calc} / (mg g^{-1})	k_1 / (h^{-1})	k_2 / (g mg^{-1} h^{-1})	h / (mg g^{-1} h^{-1})
LNB (10 mg L^{-1})	PFO	0.4496	7.23 ± 0.20	4.88	0.19	–	–
	PSO	0.9999		7.39	–	0.18	10.0
LNB (25 mg L^{-1})	PFO	0.8716	18.96 ± 0.32	13.15	0.15	–	–
	PSO	0.9611		20.23	-	0.02	8.2
LNMB (10 mg L^{-1})	PFO	0.1481	9.61 ± 0.30	0.59	0.78	–	–
	PSO	0.9999		9.61	–	9.246	854.7
LNMB (1376 mg L^{-1})	PFO	0.9323	979 ± 7	545.13	0.24	–	–
	PSO	0.9974		1000.13	–	0.002	1567.4
CAC (10 mg L^{-1})	PFO	0.1337	9.91 ± 0.20	0.79	0.07	–	–
	PSO	0.9999		9.91	–	6.058	595.2
CAC (376 mg L^{-1})	PFO	0.9486	190 ± 3	125.27	0.20	–	–
	PSO	0.9958		194.55	–	0.006	206.6

PFO: pseudo-first-order; PSO: pseudo-second-order; LNB: licuri nutshell biochar; LNMB: licuri nutshell modified biochar; CAC: commercial activated carbon; R^2: adjustment to the models; q_e: adsorptive capacity at equilibrium; q_{calc}: calculated adsorption capacity; k_1: pseudo- first-order adsorption rate constant, k_2: pseudo-second-order adsorption rate constant; h: adsorption rate.

Effect of pH in methylene blue adsorption

The pH of an aqueous medium is known for significantly influencing the materials' surface charge. In this context, pH surface charge and its effect were studied as MB is a cationic dye, and electrostatic effects could change the adsorption capacity.[85] Figure 5a shows that LNB and CAC have the same pattern of MB adsorption increasing as the pH increases from 3 to 10, while LNMB has a maximum adsorption capacity at pH = 6. This pattern can be supported by the zeta potential in Figure 5b. LNB and CAC tend to increase the negative surface charge as the pH increases, enhancing the electrostatic attraction between negative charges on the material surface by the cationic MB.[86] In the case of LNMB, the peak of negative charge (–55 mV) is found between pH 5 and 6. Meanwhile, LNB and CAC have a zeta potential of –31 and –21 mV at pH = 6, respectively. This difference in the zeta potential value can be associated with the acid and basic groups on the material's surface. For example, carboxylic or phenolic groups dissociate, releasing H^+ in water and increasing the negative charge in the functional group surroundings. In contrast, the basic groups assume a positive charge when dissociating.[46] Considering this effect, the following adsorption studies were performed at pH = 6, the pH where the materials have a negative charge density on the surface, and the pH of MB solutions without adjustments.[87]

Effect of initial dye concentration and isotherm studies

A preliminary experiment (Figure 6a) was performed to study the difference in the adsorptive capacity of the biochars at lower concentrations (0.5-14 mg L^{-1}). LNB showed a q_e of 5.29 ± 0.52 mg g^{-1} at the C_0 = 7.50 mg L^{-1}. However, this value decreased as the MB concentrations increased in the reaction medium, which might be associated with its textural properties, such as a small number of pores and the amount of dye in the media that hinders the adsorption.[88] The LNMB presented a good MB removal for all concentrations, thus suggesting that the chemical treatment was an effective process essential to improving MB adsorption. Afterward, a study was carried out at higher concentrations of MB (10-1187 mg L^{-1}) (Figure 6b) for the LNMB and CAC. These materials presented a similar adsorption profile up to the concentration of 108 mg L^{-1}, but when the initial concentration exceeds 331 mg L^{-1}, a differentiation between the adsorption capacity of these materials was noted. At C_0 = 1187 mg L^{-1}, CAC reached a maximum q_e = 141.57 mg g^{-1} while LNMB displayed a marked higher value, q_e = 808.28 mg g^{-1}.

To evaluate the adsorption equilibrium, the isotherms of the linearized Freundlich and Langmuir models were considered (Tables 4 and S6, and Figure S6, SI section).

These models make assumptions regarding the adsorbent properties, such as the shape of the isotherm and its surface nature. The Freundlich isotherm assumes a heterogeneous surface with a non-uniform adsorption energy distribution. On the other hand, the Langmuir isotherm assumes that the surface of the materials has a fixed and uniform number of active sites, and the adsorption process is reversible in front of specific stimuli and only occurs in monolayers.[48] Nevertheless, it is essential to note that each surface site may have a different interaction mode that does not affect the others. This suggests that different adsorption mechanisms can occur simultaneously but in different sites. From the adjustment to the models values, it can be seen that all materials (LNB, LNMB, and CAC) presented a profile closer to the Langmuir model, which corroborates some modified biochars reported in the literature.[84,89,90] It is worth mentioning that the q_{max} obtained by this model was closer to the q_e obtained experimentally, confirming the correct modeling of the studied biochars.

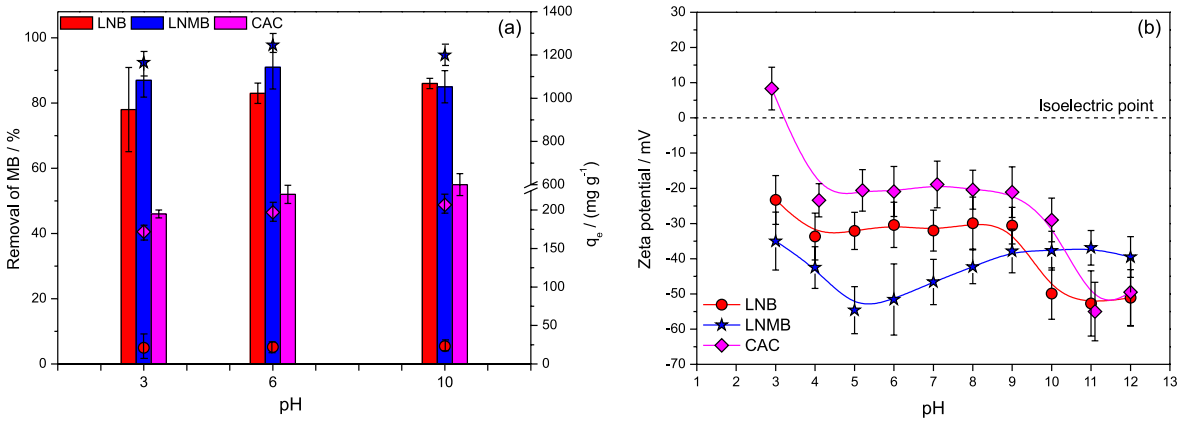

Figure 5. (a) Comparison of adsorptive capacity of materials in MB solutions at 25, 376, and 1376 mg L^{-1} for LNB, LNMB, and CAC, respectively, after 24 h in the pH of 3, 6, and 10. Conditions: mass of adsorbent = 10 mg, volume of dye solution = 10 mL (dosage 1 g L^{-1}), T = 20 °C, pH = 3, 6, and 10, and 150 rpm. Bar represents the left Y axis, and colored symbols represent the right Y axis. (b) Comparison between pH curves in the zeta potential function for all adsorbents.

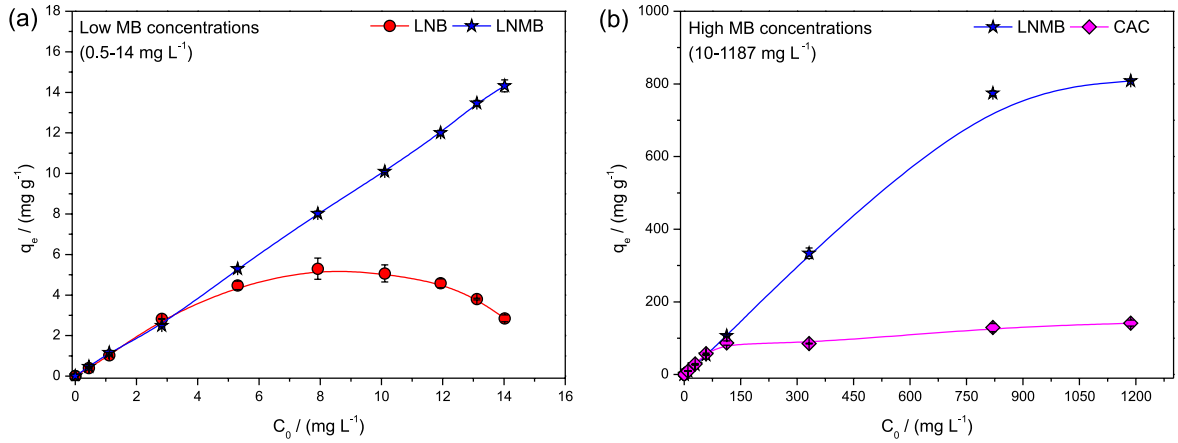

Figure 6. (a) Preliminary experiment-comparison of MB adsorptive capacity in solutions from 0.5 to 14 mg L^{-1} after 24 h. (b) Comparison of MB adsorptive capacity in solutions from 10 to 1187 mg L^{-1} after 24 h. Conditions: mass of adsorbent = 10 mg, volume of dye solution = 10 mL (dosage 1 g L^{-1}), T = 20 °C, pH = 6, and 150 rpm.

Table 4. Results of linear isotherm models applied to the chars used after 24 h of MB adsorption

Sample	Isotherm model	R^2	q_{max} / (mg g^{-1})	q_e / (mg g^{-1})	K_L / (L mg^{-1})	K_F / (mg g^{-1})	n
LNB	Langmuir	0.9868	5.27	5.29	3.801	–	–
	Freundlich	0.6276	–		–	3.49	0.443
LNMB	Langmuir	0.9990	826.45	808.28	0.167	–	––
	Freundlich	0.5102	–		–	129.09	0.364
CAC	Langmuir	0.9628	142.86	141.57	0.023	–	–
	Freundlich	0.7278	–		–	68.95	0.084

LNB: licuri nutshell biochar; LNMB: licuri nutshell modified biochar; CAC: commercial activated carbon; R^2: adjustment to the models; q_e: adsorptive capacity at equilibrium; q_{calc}: calculated adsorption capacity; k_1: pseudo- first-order adsorption rate constant, k_2: pseudo-second-order adsorption rate constant; h: adsorption rate.

Table 5 provides a comparative analysis between the materials synthesized in this study and those commonly found in the literature. The results demonstrate the superior adsorptive capacity of the LNMB, which is the only one that presented a modified structure with acid and basic active sites. Notably, this chemically treated material exhibits remarkable adsorption performance and reaches an impressive value of 826.45 mg g^{-1}. In this sense, it is worth mentioning that even when compared to materials subjected to separated acidic or basic treatments, the LNMB biochar stands out as a highly innovative and efficient adsorbent.

Recyclability and post-adsorption characterization

The recyclability study was made to ensure that the produced adsorbents could be desorbed to have at least more than one cycle of adsorption/desorption. Based on Figure 7a, it can be seen that all materials lose their removal efficiency. In the 1st cycle, LNMB has a q_e = 969 mg g^{-1}, and after the recycling process, its removal capacity reduces to q_e = 192 and 112 mg g^{-1} in the 2nd and 3rd cycles, respectively. The decrease in the adsorption capacity of LNB and CAC was not so abrupt, but even with this, their adsorption capacity remains lower than a 3rd cycle LNMB. One of the reasons that may be associated with this activity reduction is that all MB adsorbed on the 1st cycle could not be desorbed, blocking the active sites.[83] Besides the desorption washing process with ethanol being effective to other types of biochar, due to the high adsorption capacity of LNMB, other washing procedures could be tested to guarantee the complete desorption of MB molecules.[98,99] However, additional characterization would be suitable to ensure that the surface nature of the biochar would not be changed regarding acid or alkali regeneration agents.

In Figure 7b, a post-adsorption FTIR was made to see functional group changes. As it was expected, the spectra showed differences in some bands, such as the shift from 2973 and 2883 cm^{-1} to 2917 and 2846 cm^{-1} related to the C–H bond, probably due to the four $–CH_3$ in each MB molecule adsorbed. The other intensity changes in vibrational bands of C=O, C=C, and C–O bonds strongly correlate to the surface functional group acting in adsorption.[83,100] An additional remark must be made to CAC because minor changes can be seen in the material FTIR spectrum, probably because it is a pore-driven MB adsorption and fewer forces of functional groups are

Table 5. Comparative of the monolayer maximum adsorptive capacity of methylene blue (MB) with literature materials

Material	Modification agent	Method	Surface area / (m^2 g^{-1})	q_{max} / (mg g^{-1})	Temperature / °C	pH	Reference
Licuri nutshell biochar	N/A	slow pyrolysis	< 2	5.27	20 ± 2	6.0	this work
Licuri nutshell modified biochar	H_2SO_4	impregnation at 185 °C	< 2	826.45	20 ± 2	6.0	this work
Commercial activated carbon	–	–	645.9	142.86	20 ± 2	6.0	this work
Licuri nutshell fibers	N/A	N/A	–	36.40	25	5.5	91
Sugarcane filter cake biochar	N/A	slow pyrolysis	19.8	54.64	25	6.2	92
Activated banana peel	NaOH	N/A	–	19.90	20	5.0	14
Pine-fruit shell	N/A	N/A	63.7	252.00	25	8.5	93
Treated pine-fruit shell	H_2SO_4	impregnation at 100 °C	702	529.00	25	8.5	93
Cotton stalk	N/A	N/A	–	147.06	25 ± 2	7.0	94
Sulfuric acid-treated cotton stalk	H_2SO_4	impregnation at 150 °C	2.8	555.56	25 ± 2	7.0	94
Phosphoric acid-treated cotton stalk	H_3PO_4	impregnation at 150 °C	7.3	222.22	25 ± 2	7.0	94
Activated bamboo dust biochar	–	carbonization, steam digestion, and acid treatment	–	143.20	30 ± 1	7.2	16
Activated coconut shell biochar	–		–	277.90	30 ± 1	7.2	16
Activated rice husk biochar	–		–	164.90	30 ± 1	7.2	16
Activated periwinkle shell biochar	KOH	pyrolysis	–	500.00	25 ± 1	7.0	95
Activated beer residue biochar	CO_2	pyrolysis and CO_2 activation	80.5	161.00	25	6.5	96
Treated coconut shell	H_2SO_4	impregnation at 150 °C	< 2	50.60	30	8	97

N/A: not applied.

used (no acid sites and low basic sites, Table 2). Also, the micrographs presented in Figure S7 (SI section) illustrate the distinctive characteristics of the adsorbents before and after MB adsorption. Remarkably, the adsorption process does not induce significant morphological alterations. However, discernible surface agglomerates are observed. Particularly noteworthy is the LNMB, which has the highest adsorption capacity wherein the degree of aggregation appears to be more pronounced.

However, despite the deactivation of the LNMB material, it is essential to mention that it represents a step forward in preparing more sustainable adsorbents for dyes-polluted wastewater. The adsorption and reuse of the CAC were superior or comparable, but the industrial production of activated carbon involves several energy-demanding steps and generates waste.[101] For example, CACs are typically produced under an inert atmosphere at temperatures ranging from 600 to 900 °C, exposed to strong bases (e.g., KOH) in

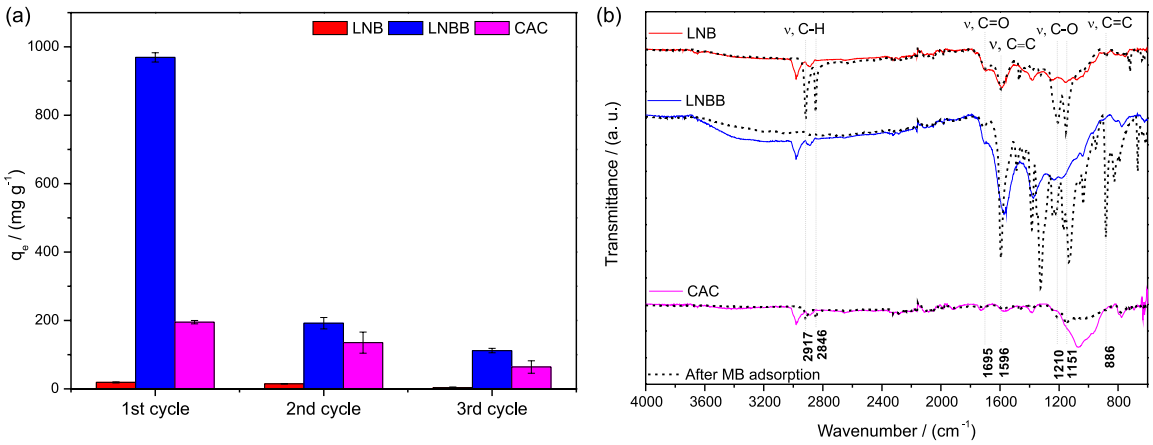

Figure 7. (a) Comparison of the recyclability of the produced materials applied to MB removal. [MB] = 25, 376, and 1376 mg L^{-1} for LNB, LNMB, and CAC. Conditions: mass of adsorbent = 10 mg, volume of dye solution = 10 mL (dosage 1 g L^{-1}), T = 20 °C, pH = 6, 150 rpm, and contact time = 24 h. (b) Normalized FTIR spectra of the materials before and after the MB adsorption (1st cycle).

large amounts for pore creation, followed by other thermal activation steps to develop porosity.[102] In this sense, LNMB production is greener because it uses a lignocellulosic biomass residue, and its modification processes are milder. Furthermore, from a sustainable point of view, it is also possible to recover the acid and basic solutions and employ them to produce other batches.[103] Besides, our biochar LNMB was able to remove in a single adsorption cycle almost 2.5 times more MB than CAC in three adsorption cycles, i.e., q_e 969 mg g^{-1} *versus* 394 mg g^{-1}.

Methylene blue adsorption mechanism

An overall comparison between the adsorption capacity and the physicochemical properties of the biochar materials reveals that multiple processes could be related to the high adsorption capacity of the LNMB sample, including chemisorption and physisorption mechanisms.[84] The chemical treatment with acid and base increased the total acidic and basic groups and formed oxygenated surface functional groups, confirmed by Boehm titration and FTIR. As shown in Figure 8, the functionalized surface of the biochar can exert a crucial role in MB adsorption. In Figure 8a, some oxygenated functional groups on the surface of the material are responsible for hydrogen bonding with the N atom of the MB with the carbonaceous adsorbent, thus improving its removal.[104] In addition, the interaction of π-electrons of MB aromatic rings and the π-electrons from the biochar aromatic structure might lead to a π-π stacking interaction (Figure 8b). In Figure 8c, when the pH > pH_{PZC}, the net surface of the material is negatively charged (i.e., occurring the deprotonation of functional groups), hence favoring an electrostatic attraction with positively charged species, such as MB (cationic dye).[105] In Figure 8d, although the textural properties of LNB and LNMB were relatively low (compared to conventional adsorbents such as CAC) to support strong physisorption into the pores, this process must be considered. In Figure 8e, the cationic exchange process is shown, which can occur by the inorganic composition (metal ions or ash content) of the biochar and the MB. In the case of LNMB, this mechanism was probably enhanced due to the insertion of $–O^-Na^+$ sites in the washing step with sodium hydroxide.[79] All these phenomena support that despite the low surface area of LNMB, this biochar still had a high adsorption capacity and confirmed that the adsorption process is not only ruled by the presence of highly porous materials. This observation was also recently reported by Jawad *et al.*[97] and Zhu *et al.*,[106] where H_2SO_4-treated biomass and slow pyrolysis biochars with low porosity characteristics exhibited an enhanced adsorption capacity towards MB. In contrast, CAC was the only material with a dominating porosity role in the adsorption mechanism, probably because of a lower quantity of functional groups detected by FTIR and Boehm titration.

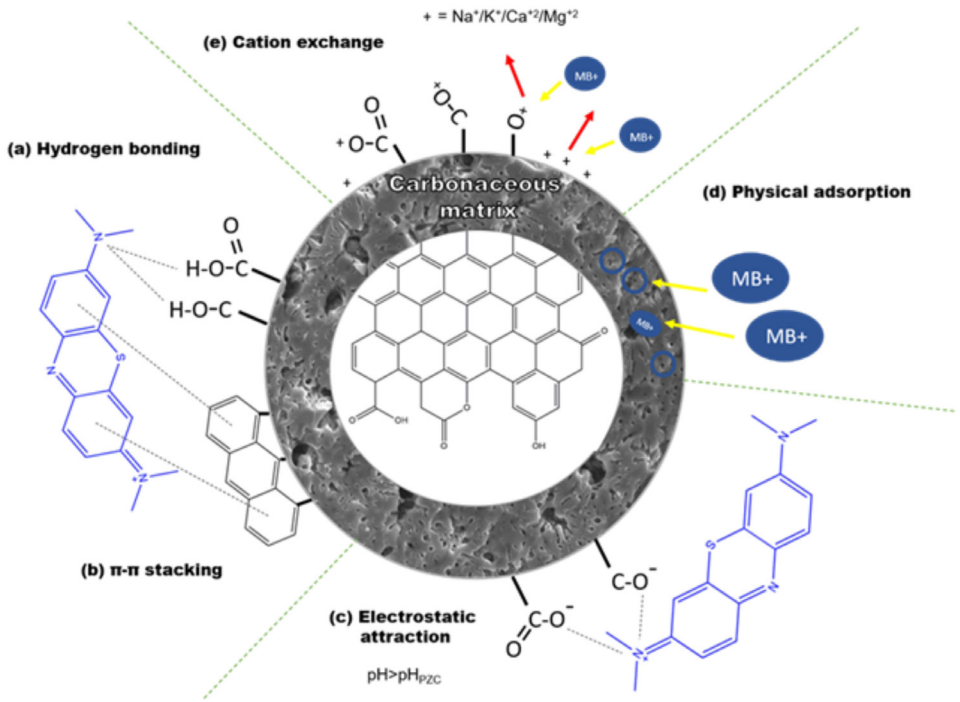

Figure 8. Proposed adsorption mechanisms of MB over LNMB biochar.

Conclusions

This study successfully demonstrated the conversion of licuri nutshell (a Brazilian lignocellulosic waste) into biochar with high economic value and improved adsorption properties. Through slow pyrolysis, substantial yields of biochar (36%), bio-oil (9%), aqueous fraction (31%), and gas (24%) were obtained. The subsequent chemical treatment of licuri nutshell biochar with sulfuric acid and sodium hydroxide generated acid and basic sites, resulting in a remarkable 155-fold increase in the adsorption capacity for MB compared to its precursor biochar. This chemical modification effectively transformed the residual biochar into a product that surpassed commercial coal and other biochar and biomass reported in the literature. Moreover, the Langmuir isotherm and PSO kinetics models were the most appropriate fit between the different models. Notably, the investigation of adsorption mechanisms revealed the prominent roles of surface functional groups and electrostatic forces, highlighting their significance over material low porosity. In summary, this work presents a groundbreaking contribution by successfully converting licuri nutshell waste into high-value biochar with enhanced adsorption capabilities.

Supplementary Information

Supplementary information (TGA analyses, N_2 adsorption isotherms, and other MB adsorption data) is free of charge at http://jbcs.sbq.org.br as PDF file.

Acknowledgments

This work was supported by the Fundação Carlos Chagas Filho de Amparo à Pesquisa do Estado do Rio de Janeiro (FAPERJ process No. E-26/200.174/2018; E-26/211.575/2019; E-26/201.358/2021; E-26/210.315/2022), by the Coordenação de Aperfeiçoamento de Pessoal de Nível Superior (CAPES) and the Conselho Nacional de Desenvolvimento Científico e Tecnológico (CNPq). This study was financed in part by the Coordenação de Aperfeiçoamento de Pessoal de Nível Superior - Brasil (CAPES) - Finance Code 00.

Author Contributions

Gustavo F. Bitencourt was responsible for conceptualization, data curation, formal analysis, investigation, methodology, resources, validation, and writing (original draft, review and editing); Letícia F. L. Machado for investigation and methodology; Bruno S. Peixoto for conceptualization, supervision, methodology, and writing (review and editing); Laís F. de Castro for conceptualization, methodology, resources, project administration, supervision, and writing (review and editing); Márcia C. C. Veloso for resources, methodology, supervision, and funding acquisition; Gilberto A.Romeiro for resources, methodology, supervision, and funding acquisition; Thiago M. Lima for resources, methodology, supervision, funding acquisition, writing (review and editing).

References

1. Wang, B.; Lee, X.; Theng, B. K. G.; Zhang, L.; Cheng, H.; Cheng, J.; Lyu, W.; *Environ. Pollut. Bioavailability* **2019**, *31*, 38. [Crossref]
2. Luo, L.; Wang, X.; Guo, H.; *Innovation* **2022**, *3*, 100227. [Crossref]
3. Burkinshaw, S. M.; Salihu, G.; *Dyes Pigm.* **2013**, *99*, 548. [Crossref]
4. Ghazi Mokri, H. S.; Modirshahla, N.; Behnajady, M. A.; Vahid, B.; *Int. J. Environ. Sci. Technol.* **2015**, *12*, 1401. [Crossref]
5. Praveen, S.; Jegan, J.; Bhagavathi Pushpa, T.; Gokulan, R.; Bulgariu, L.; *Biochar* **2022**, *4*, 10. [Crossref]
6. Honorato, A. C.; Machado, J. M.; Celante, G.; Borges, W. G. P.; Dragunski, D. C.; Caetano, J.; *Rev. Bras. Eng. Agric. Ambient.* **2015**, *19*, 705. [Crossref]
7. Khan, I.; Saeed, K.; Zekker, I.; Zhang, B.; Hendi, A. H.; Ahmad, A.; Ahmad, S.; Zada, N.; Ahmad, H.; Shah, L. A.; Shah, T.; Khan, I.; *Water* **2022**, *14*, 242. [Crossref]
8. Perlberg, S. T.; Diamant, A.; Ofir, R.; Zilberg, D.; *J. Fish Dis.* **2008**, *31*, 215. [Crossref]
9. Ghosh, D.; Bhattacharyya, K. G.; *Appl. Clay Sci.* **2002**, *20*, 295. [Crossref]
10. Supelano, G. I.; Gómez Cuaspud, J. A.; Moreno-Aldana, L. C.; Ortiz, C.; Trujillo, C. A.; Palacio, C. A.; Parra Vargas, C. A.; Mejía Gómez, J. A.; *Fuel* **2020**, *263*, 116800. [Crossref]
11. Soni, S.; Bajpai, P. K.; Mittal, J.; Arora, C.; *J. Mol. Liq.* **2020**, *314*, 113642. [Crossref]
12. Li, Y.; Du, Q.; Liu, T.; Peng, X.; Wang, J.; Sun, J.; Wang, Y.; Wu, S.; Wang, Z.; Xia, Y.; Xia, L.; *Chem. Eng. Res. Des.* **2013**, *91*, 361. [Crossref]
13. Al-Qodah, Z.; Shawabkah, R.; *Braz. J. Chem. Eng.* **2009**, *26*, 127. [Crossref]
14. Amel, K.; Hassen, M. A.; Kerroum, D.; *Energy Procedia* **2012**, *19*, 286. [Crossref]
15. Bernardino, C. A. R.; Mahler, C. F.; Veloso, M. C. C.; Romeiro, G. A.; *Waste Biomass Valorization* **2017**, *8*, 2511. [Crossref]
16. Kannan, N.; Sundaram, M. M.; *Dyes Pigm.* **2001**, *51*, 25. [Crossref]
17. Lorenzi, H.; Souza, H. M.; Medeiros-Costa, J. T.; Cerqueira, L. S. C.; Ferreira, E.; *Palmeiras Brasileiras e Exóticas Cultivadas*; Instituto Plantarum: Nova Odessa, Brazil, 2004.
18. Crepaldi, I. C.; Almeida-Muradian, L. B.; Rios, M. D. G.; Penteado,

M. V. C.; Salatino, A.; *Braz. J. Bot.* **2001**, *24*, 155. [Crossref]
19. Rufino, M. U. L.; Costa, J. T. M.; da Silva, V. A.; Andrade, L. H. C.; *Acta Bot. Bras.* **2009**, *22*, 1141. [Crossref]
20. Aroucha, E. P. T. L.; Aroucha, M. L.; *Boas Práticas de Manejo para o Extrativismo Sustentável do Licuri*; Instituto Sociedade, População e Natureza: Brasília, Brazil, 2013.
21. Uddin, M. N.; Techato, K.; Taweekun, J.; Rahman, M. M.; Rasul, M. G.; Mahlia, T. M. I.; Ashrafur, S. M.; *Energies* **2018**, *11*, 3115. [Crossref]
22. Bridgwater, A. V.; *Biomass Bioenergy* **2012**, *38*, 68. [Crossref]
23. Bridgwater, A. V.; Grassi, G.; *Biomass Pyrolysis Liquids Upgrading and Utilization*, 1st ed.; Elsevier: New York, USA, 1991. [Crossref]
24. Lehmann, J.; Joseph, S.; *Biochar for Environmental Management*, 2nd ed.; Routledge: London, UK, 2015. [Crossref]
25. Din, M. I.; Ashraf, S.; Intisar, A.; *Sci. Prog.* **2017**, *100*, 299. [Crossref]
26. Sevilla, M.; Díez, N.; Fuertes, A. B.; *ChemSusChem* **2021**, *14*, 94. [Crossref]
27. Gomes, H. T.; Miranda, S. M.; Sampaio, M. J.; Silva, A. M. T.; Faria, J. L.; *Catal. Today* **2010**, *151*, 153. [Crossref]
28. Abdullah, R. F.; Rashid, U.; Ibrahim, M. L.; Nolhakim, M. A. H. L.; Moser, B. R.; Alharthi, F. A.; *Process Saf. Environ. Prot.* **2021**, *156*, 219. [Crossref]
29. Bounoukta, C. E.; Megías-Sayago, C.; Navarro, J. C.; Ammari, F.; Ivanova, S.; Centeno, M. Á.; Odriozola, J. A.; *Nanomaterials* **2023**, *13*, 1129. [Crossref]
30. Liao, Y.; Chen, S.; Zheng, Q.; Huang, B.; Zhang, J.; Fu, H.; Gao, H.; *Inorg. Chem. Commun.* **2022**, *139*, 109341. [Crossref]
31. Uddin, M. K.; *Chem. Eng. J.* **2017**, *308*, 438. [Crossref]
32. Gaunt, J. L.; Lehmann, J.; *Environ. Sci. Technol. Sci. Technol.* **2008**, *42*, 4152. [Crossref]
33. Peters, J. F.; Iribarren, D.; Dufour, J.; *Environ. Sci. Technol.* **2015**, *49*, 5195. [Crossref]
34. Choudhary, V.; Philip, L.; *J. Environ. Chem. Eng.* **2022**, *10*, 107592. [Crossref]
35. Schroeder, P.; do Nascimento, B. P.; Romeiro, G. A.; Figueiredo, M. K. K.; Veloso, M. C. C.; *J. Anal. Appl. Pyrolysis* **2017**, *124*, 161. [Crossref]
36. Silva, R. V. S.; Gonçalves, A. D.; Vinhal, J. O.; Cassella, R. J.; Santos, R. C.; Dal Sasso, M. A.; Peixoto, B. S.; Borba-Santos, L. P.; Rozental, S.; Azevedo, D. A.; Romeiro, G. A.; *J. Environ. Chem. Eng.* **2021**, *9*, 104825. [Crossref]
37. David, E.; Kopac, J.; *J. Anal. Appl. Pyrolysis* **2014**, *110*, 322. [Crossref]
38. ASTM D1762-84: *Standard Test Method for Chemical Analysis of Wood Charcoal*, West Conshohocken, 2013.
39. ASTM D3172-13: *Standard Practice for Proximate Analysis of Coal and Coke*, West Conshohocken, 2013.
40. Pucciariello, R.; D'Auria, M.; Bonini, C.; Vetere, T.; Villani, V.; *Polymer* **2004**, *45*, 4159. [Crossref]
41. Rasband, W. S.; *ImageJ*, version 1; U. S. National Institutes of Health, Bethesda, Maryland, USA, 1997.
42. Negara, D. N. K. P.; Nindhia, T. G. T.; Surata, I. W.; Hidajat, F.; Sucipta, M.; *Mater. Today Proc.* **2020**, *22*, 148. [Crossref]
43. Li, B.; Yang, L.; Wang, C.-Q; Zhang, Q. P.; Liu, Q. C.; Li, Y. D.; Xiao, R.; *Chemosphere* **2017**, *175*, 332. [Crossref]
44. Nnaji, N. J. N.; Sonde, C. U.; Nwanji, O. L.; Ezeh, G. C.; Onuigbo, A. U.; Ojukwu, A. M.; Mbah, P. C.; Adewumi, A. O.; Unoka, E. C.; Otedo, J. O.; Onuegbu, T. U.; *J. Environ. Chem. Eng.* **2023**, *11*, 109638. [Crossref]
45. Labuto, G.; Carvalho, A. P.; Mestre, A. S.; dos Santos, M. S.; Modesto, H. R.; Martins, T. D.; Lemos, S. G.; da Silva, H. D. T.; Carrilho, E. N. V. M.; Carvalho, W. A.; *Sustainable Chem. Pharm.* **2022**, *28*, 100703. [Crossref]
46. Yuan, J.-H.; Xu, R.-K.; *Soil Use Manage.* **2011**, *27*, 110. [Crossref]
47. Güleç, F.; Williams, O.; Kostas, E. T.; Samson, A.; Stevens, L. A.; Lester, E.; *Energy Convers. Manage.* **2022**, *270*, 116260. [Crossref]
48. Tran, H. N.; You, S.-J.; Hosseini-Bandegharaei, A.; Chao, H.-P.; *Water Res.* **2017**, *120*, 88. [Crossref]
49. Blanchard, G.; Maunaye, M.; Martin, G.; *Water Res.* **1984**, *18*, 1501. [Crossref]
50. Ho, Y.-S.; *J. Hazard. Mater.* **2006**, *136*, 681. [Crossref]
51. Ho, Y. S.; McKay, G.; *Process Saf. Environ. Prot.* **1998**, *76*, 332. [Crossref]
52. Mu, Y.; Ma, H.; *Chem. Eng. Res. Des.* **2021**, *167*, 129. [Crossref]
53. Bessa, C. M. A. S.; do Nascimento, R. S.; Alves, R. C. C.; Anselmo, J. M.; da Silva, A. P. S.; da Silva, A. G.; Lima, V. L. M.; Tavares, J. F.; da Silva, L. C. N.; Silva, M. V.; Correia, M. T. S.; *J. Med. Plants Res.* **2016**, *10*, 310. [Crossref]
54. Iha, O. K.; Alves, F. C. S. C.; Suarez, P. A. Z.; de Oliveira, M. B. F.; Meneghetti, S. M. P.; Santos, B. P. T.; Soletti, J. I.; *Ind. Crops Prod.* **2014**, *62*, 318. [Crossref]
55. Mattos, C.; Veloso, M. C. C.; Romeiro, G. A.; Folly, E.; *J. Anal. Appl. Pyrolysis* **2019**, *139*, 1. [Crossref]
56. Xiao, X.; Chen, Z.; Chen, B.; *Sci. Rep.* **2016**, *6*, 226644. [Crossref]
57. Collard, F.-X.; Blin, J.; *Renewable Sustainable Energy Rev.* **2014**, *38*, 594. [Crossref]
58. Qian, K.; Kumar, A.; Patil, K.; Bellmer, D.; Wang, D.; Yuan, W.; Huhnke, R. L.; *Energies* **2013**, *6*, 3972. [Crossref]
59. Sharma, R. K.; Wooten, J. B.; Baliga, V. L.; Lin, X.; Chan, W. G.; Hajaligol, M. R.; *Fuel* **2004**, *83*, 1469. [Crossref]
60. Chen, H.; Wang, Y.; Xu, G.; Yoshikawa, K.; *Energies* **2012**, *5*, 5418. [Crossref]
61. Thomas, E.; Borchard, N.; Sarmiento, C.; Atkinson, R.; Ladd, B.; *Biochar* **2020**, *2*, 151. [Crossref]
62. Gwenzi, W.; Chaukura, N.; Wenga, T.; Mtisi, M.; *Sci. Total Environ.* **2021**, *753*, 142249. [Crossref]

63. Demirbas, A.; *Energy Explor. Exploit.* **2002**, *20*, 105. [Crossref]
64. Niu, T.; Zhou, J.; Zhang, C.; Li, S.; *RSC Adv.* **2018**, *8*, 26978. [Crossref]
65. Tellez-Juárez, M. C.; Fierro, V.; Zhao, W.; Fernández-Huerta, N.; Izquierdo, M. T.; Reguera, E.; Celzard, A.; *Int. J. Hydrogen Energy* **2014**, *39*, 4996. [Crossref]
66. de Mendonça, F. G.; da Cunha, I. T.; Soares, R. R.; Tristão, J. C.; Lago, R. M.; *Bioresour. Technol.* **2017**, *246*, 28. [Crossref]
67. Salleh, M. A. M.; Mahmoud, D. K.; Karim, W. A. W. A.; Idris, A.; *Desalination* **2011**, *280*, 1. [Crossref]
68. Yaseen, D. A.; Scholz, M.; *Int. J. Environ. Sci. Technol.* **2019**, *16*, 1193. [Crossref]
69. Zhao, S. X.; Ta, N.; Wang, X. D.; *Energies* **2017**, *10*, 1293. [Crossref]
70. Guo, J.; Xu, W. S.; Chen, Y. L.; Lua, A. C.; *J. Colloid Interface Sci.* **2005**, *281*, 285. [Crossref]
71. Iriarte-Velasco, U.; Ayastuy, J. L.; Zudaire, L.; Sierra, I.; *Chem. Eng. J.* **2014**, *251*, 217. [Crossref]
72. Liu, C.; Wang, W.; Wu, R.; Liu, Y.; Lin, X.; Kan, H.; Zheng, Y.; *ACS Omega* **2020**, *5*, 30906. [Crossref]
73. Bedin, K. C.; Martins, A. C.; Cazetta, A. L.; Pezoti, O.; Almeida, V. C.; *Chem. Eng. J.* **2016**, *286*, 476. [Crossref]
74. Tomczyk, A.; Sokołowska, Z.; Boguta, P.; *Rev. Environ. Sci. Biotechnol.* **2020**, *19*, 191. [Crossref]
75. Ramirez-Gutierrez, C. F.; Arias-Niquepa, R.; Prías-Barragán, J. J.; Rodriguez-Garcia, M. E.; *J. Environ. Chem. Eng.* **2020**, *8*, 103636. [Crossref]
76. Peixoto, B. S.; Mota, L. S. O.; de Oliveira, P. C. O.; Veloso, M. C. C.; Romeiro, G. A.; de Moraes, M. C.; *Water* **2022**, *14*, 3525. [Crossref]
77. Jindo, K.; Mizumoto, H.; Sawada, Y.; Sanchez-Monedero, M. A.; Sonoki, T.; *Biogeosciences* **2014**, *11*, 6613. [Crossref]
78. Thommes, M.; Kaneko, K.; Neimark, A. V.; Olivier, J. P.; Rodriguez-Reinoso, F.; Rouquerol, J.; Sing, K. S. W.; *Pure Appl. Chem.* **2015**, *87*, 1051. [Crossref]
79. Valencia, A.; Muñiz-Valencia, R.; Ceballos-Magaña, S. G.; Rojas-Mayorga, C. K.; Bonilla-Petriciolet, A.; González, J.; Aguayo-Villarreal, I. A.; *Environ. Technol. Innov.* **2022**, *25*, 102076. [Crossref]
80. Zhou, Z.; Yao, D.; Li, S.; Xu, F.; Liu, Y.; Liu, R.; Chen, Z.; *Environ. Technol. Innov.* **2021**, *24*, 102025. [Crossref]
81. Hafizuddin, M. S.; Lee, C. L.; Chin, K. L.; H'ng, P. S.; Khoo, P. S.; Rashid, U.; *Polymers* **2021**, *13*, 3954. [Crossref]
82. Saleh, T. A.; Danmaliki, G. I.; *J. Taiwan Inst. Chem. Eng.* **2016**, *60*, 460. [Crossref]
83. Sh. Gohr, M.; Abd-Elhamid, A. I.; El-Shanshory, A. A.; Soliman, H. M. A.; *J. Mol. Liq.* **2022**, *346*, 118227. [Crossref]
84. Pandey, D.; Daverey, A.; Dutta, K.; Yata, V. K.; Arunachalam, K.; *Environ. Technol. Innov.* **2022**, *25*, 102200. [Crossref]
85. Li, H.; Budarin, V. L.; Clark, J. H.; North, M.; Wu, X.; *J. Hazard. Mater.* **2022**, *436*, 129174. [Crossref]
86. Hsu, D.; Lu, C.; Pang, T.; Wang, Y.; Wang, G.; *Appl. Sci.* **2019**, *9*, 5249. [Crossref]
87. Prahas, D.; Kartika, Y.; Indraswati, N.; Ismadji, S.; *Chem. Eng. J.* **2008**, *140*, 32. [Crossref]
88. do Nascimento, G. E.; Duarte, M. M. M. B.; Campos, N. F.; da Rocha, O. R. S.; da Silva, V. L.; *Environ. Technol.* **2014**, *35*, 1436. [Crossref]
89. Quansah, J. O.; Hlaing, T.; Lyonga, F. N.; Kyi, P. P.; Hong, S. H.; Lee, C. G.; Park, S. J.; *Appl. Sci.* **2020**, *10*, 3437. [Crossref]
90. Ma, Z. W.; Zhang, K. N.; Zou, Z. J.; Lü, Q. F.; *J. Environ. Chem. Eng.* **2021**, *9*, 105251. [Crossref]
91. Meili, L.; da Silva, T. S.; Henrique, D. C.; Soletti, J. I.; de Carvalho, S. H. V.; da Silva Fonseca, E. J.; de Almeida, A. R. F.; Dotto, G. L.; *Water Sci. Technol.* **2017**, *75*, 106. [PubMed]
92. Bernardino, C. A. R.; Mahler, C. F.; Veloso, M. C. C.; Romeiro, G. A.; Schroeder, P.; *Rev. Virtual Quim.* **2018**, *10*, 551. [Crossref]
93. Royer, B.; Cardoso, N. F.; Lima, E. C.; Vaghetti, J. C. P.; Simon, N. M.; Calvete, T.; Veses, R. C.; *J. Hazard. Mater.* **2009**, *164*, 1213. [Crossref]
94. Deng, H.; Lu, J.; Li, G.; Zhang, G.; Wang, X.; *Chem. Eng. J.* **2011**, *172*, 326. [Crossref]
95. Bello, O. S.; Adeogun, I. A.; Ajaelu, J. C.; Fehintola, E. O.; *Chem. Ecol.* **2008**, *24*, 285. [Crossref]
96. Franciski, M. A.; Peres, E. C.; Godinho, M.; Perondi, D.; Foletto, E. L.; Collazzo, G. C.; Dotto, G. L.; *Waste Manage.* **2018**, *78*, 630. [Crossref]
97. Jawad, A. H.; Abdulhameed, A. S.; Mastuli, M. S.; *J. Taibah Univ. Sci.* **2020**, *14*, 305. [Crossref]
98. Song, G.; Guo, Y.; Li, G.; Zhao, W.; Yu, Y.; *Desalin. Water Treat.* **2019**, *160*, 316. [Crossref]
99. Alsawy, T.; Rashad, E.; El-Qelish, M.; Mohammed, R. H.; *npj Clean Water* **2022**, *5*, 29. [Crossref]
100. Dinh, V. P.; Huynh, T. D. T.; Le, H. M.; Nguyen, V. D.; Dao, V. A.; Hung, N. Q.; Tuyen, L. A.; Lee, S.; Yi, J.; Nguyen, T. D.; Tan, L. V.; *RSC Adv.* **2019**, *9*, 25847. [Crossref]
101. Kamali, M.; Appels, L.; Kwon, E. E.; Aminabhavi, T. M.; Dewil, R.; *Chem. Eng. J.* **2021**, *420*, 129946. [Crossref]
102. Lee, H. W.; Lee, H.; Kim, Y. M.; Park, R. su; Park, Y. K.; *Chin. Chem. Lett.* **2019**, *30*, 2147. [Crossref]
103. Moreira, M. T.; Noya, I.; Feijoo, G.; *Bioresour. Technol.* **2017**, *246*, 135. [Crossref]
104. Wang, Y.; Zhang, Y.; Li, S.; Zhong, W.; Wei, W.; *J. Mol. Liq.* **2018**, *268*, 658. [Crossref]
105. Fan, S.; Wang, Y.; Wang, Z.; Tang, J.; Tang, J.; Li, X.; *J. Environ. Chem. Eng.* **2017**, *5*, 601. [Crossref]
106. Zhu, Y.; Yi, B.; Yuan, Q.; Wu, Y.; Wang, M.; Yan, S.; *RSC Adv.* **2018**, *8*, 19917. [Crossref]

Submitted: July 16, 2023
Published online: November 14, 2023